



# Molecular modeling of averaged rigor crossbridges from tomograms of insect flight muscle<sup>☆</sup>

Li Fan Chen,<sup>a,1</sup> Hanspeter Winkler,<sup>a</sup> Michael K. Reedy,<sup>b</sup> Mary C. Reedy,<sup>b</sup>  
and Kenneth A. Taylor<sup>a,\*</sup>

<sup>a</sup> *Institute of Molecular Biophysics, Florida State University, Tallahassee, FL 32306-4380, USA*

<sup>b</sup> *Department of Cell Biology, Duke University Medical Center, Durham, NC 27710, USA*

Received 7 December 2001; and in revised form 16 April 2002

## Abstract

Electron tomography, correspondence analysis, molecular model building, and real-space refinement provide detailed 3-D structures for in situ myosin crossbridges in the nucleotide-free state (rigor), thought to represent the end of the power stroke. Unaveraged tomograms from a 25-nm longitudinal section of insect flight muscle preserved native structural variation. Recurring crossbridge motifs that repeat every 38.7 nm along the actin filament were extracted from the tomogram and classified by correspondence analysis into 25 class averages, which improved the signal to noise ratio. Models based on the atomic structures of actin and of myosin subfragment 1 were rebuilt to fit 11 class averages. A real-space refinement procedure was applied to quantitatively fit the reconstructions and to minimize steric clashes between domains introduced during the fitting. These combined procedures show that no single myosin head structure can fit all the in situ crossbridges. The validity of the approach is supported by agreement of these atomic models with fluorescent probe data from vertebrate muscle as well as with data from regulatory light chain crosslinking between heads of smooth muscle heavy meromyosin when bound to actin. © 2002 Elsevier Science (USA). All rights reserved.

*Keywords:* Muscle contraction; Muscle proteins; Muscle physiology; Myosin; Actin

## 1. Introduction

The rigor state is characterized by maximization of stable attachments of nucleotide-free myosin heads to actin. In contracting muscle, this state is short lived due to the rapid binding of ATP and detachment of myosin from actin. Unlike twitch contractions, in which crossbridges detach rapidly after executing a working stroke, rigor induction involves a slower development of tension that is sustained for hours in the absence of ATP. The myosin head forms that accumulate in rigor produce tension under the local con-

straints of the filament lattice and molecular structure of two-headed myosin. This is in contrast to in vitro conditions, where myosin heads bind actin without development of tension and where rigor-bound myosin subfragment 1 (S1)<sup>2</sup> is typically described as a single, uniform structure. Insect flight muscle (IFM) rigor crossbridges provide an opportunity to study two-headed attachments while at the same time acting as a model system for the development of methods to obtain 3-D information for variable structures that are irregularly distributed in large arrays.

<sup>☆</sup> The reconstructions described in this paper have been deposited for public access in the European Bioinformatics Institute under the accession code EMD-1001.

\* Corresponding author. Fax: +850-644-7244.

E-mail address: taylor@bio.fsu.edu (K.A. Taylor).

<sup>1</sup> Present address: Read-Rite Corporation, 44100 Osgood Road, Fremont, CA 94539, USA.

<sup>2</sup> *Abbreviations used:* S1, myosin subfragment 1, the proteolytic fragment containing heavy chain residues 1–843 and the essential and regulatory light chains; ELC, essential light chain; RLC, regulatory light chain; LCD, light chain domain consisting of heavy chain residues 770–843 and both the essential and regulatory light chains; IFM, insect flight muscle; smHMM, smooth muscle heavy meromyosin.

In comparison with our previous 3-D reconstructions of rigor IFM (Taylor et al., 1984, 1989a, b, 1993), the present study implements technical and methodological advances that now allow us to infer positions of interacting loops and residues in atomic models of S1 rebuilt to fit crossbridges in lower resolution 3-D tomograms. These advances include computational identification structural classes that are representative of the crossbridge motifs extracted from electron tomograms (Winkler and Taylor, 1999). In practical terms, the approach allows us to identify variations in the characteristic “double chevron” crossbridge motif regardless of how randomly the motifs may be distributed throughout the lattice and produces class averages that preserve more crossbridge variation than the spatial averages used previously.

In order to improve on molecular models rebuilt to fit crossbridges in tomograms, we have implemented a real-space refinement protocol which quantitatively fits the density and partially corrects for residue clashes introduced during model rebuilding (Chen et al., 2001). An improved molecular model of the myosin head was thereby obtained by using several pivot points within the light chain domain (LCD) that provided a better match to the density and which had fewer interatomic clashes than the manually rebuilt models. This effort reveals axial, azimuthal, and rotational positions of rigor LCD lever arms that reflect the myosin head deformations required for attachment in the intact muscle lattice.

The novelty of our approach requires some cross-validation. The refined models described here allow comparison to data from fluorescent probes attached to the LCD domain in vertebrate muscle fibers that track active and rigor lever arm movements (Baumann et al., 2001; Corrie et al., 1999; Hopkins et al., in press). The axial, azimuthal, and twisting movements detected in these probe studies are similar to the movements of the LCD lever arm inferred from the range of positions observed in our refined models.

We can also infer the positions of specific residues in the myosin light chains in our refined models, which allows us to explore the locations of corresponding residues used in crosslinking studies. Cremo and co-workers have carried out extensive studies on the crosslinking between the RLCs on the two heads in smooth muscle heavy meromyosin (smHMM) (Wu et al., 1999). Wu et al. mutated the RLC of expressed smHMM to introduce cystein residues at various locations in order to identify potential interacting sites between the two myosin heads in the presence or the absence of RLC phosphorylation and when smHMM is bound to actin in rigor. Our models of two-headed rigor crossbridges independently confirm the same interhead site proximities, thus validating our approach for this and future work.

## 2. Methods

### 2.1. Specimen preparation

Muscle fibers were obtained from the dorsal longitudinal flight muscles of *Lethocerus maximus*. Fibers were glycerinated and prepared for electron microscopy as described (Reedy and Reedy, 1985). The particular batch of specimens was selected based on the presence of diffraction on the 5.9- and 5.1-nm layerlines of F-actin in computed transforms. Sections were judged to be ~25 nm thick based on their appearance and the known arrangement of actin and myosin filaments in IFM. Section compression in this specimen is 11% based on changes in the interfilament spacing compared to the hydrated muscle.

### 2.2. Tomographic reconstruction

Image data were obtained at a magnification 17000 $\times$  on a Philips EM420 electron microscope and consisted of a dual axis tilt series in  $\sim 10^\circ$  increments to  $\pm 60^\circ$ ; one tilt axis was parallel to the filament axis and the other at  $90^\circ$  to the filament axis. No attempt was made to minimize radiation dose. The data were digitized on a Perkin-Elmer PDS 1010M microdensitometer at a step size of 1.55 nm. The tilt series were aligned by cross-correlation analysis and combined in 3-D using methods previously described (Taylor et al., 1997). Previous reconstructions from this same specimen were spatially averaged (Taylor et al., 1984, 1989a, 1989b) and showed three very similar averaged motifs, but the present reconstruction has not been spatially averaged.

### 2.3. Multivariate statistical analysis

Three-dimensional motifs were identified in the tomogram from the centers of gravity of peaks in a cross-correlation map. We define a 3-D motif as one entire 38.7-nm repeat of attached crossbridges along actin. These motifs usually contain at least four myosin heads in two paired crossbridges (single chevrons) and sometimes contain as many as six myosin heads in four paired crossbridges (double chevrons). The reference for the analysis was selected to be centered between densities of successive troponins, which could be identified from the in-plane projection. The individual crossbridge motifs were then subjected to multivariate statistical analysis to identify clusters of motifs showing similar crossbridge structure (Frank and van Heel, 1982; van Heel and Frank, 1981). These clusters were used to form class averages.

Averaging was done according to the hierarchical ascendant method (van Heel, 1984) as detailed in Winkler and Taylor (1999). The resolution in each of the class averages was 7 nm by the spectral signal to noise

ratio (Unser et al., 1987), which was deemed the appropriate method because the limited number of motifs in each class average was too few to divide into two groups for Fourier shell correlation or differential phase residual.

#### 2.4. Model building

Three-dimensional atomic models of rigor acto-S1 were rebuilt to fit the class averages in the reconstruction using the crystallographic modeling program O (Jones et al., 1991). Eleven class averages produced a total of 58 fitted models of rigor myosin heads. For the atomic structure of actin, we used the coordinate set from Holmes et al. (1990), PDB 1ATN. For myosin subfragment 1, we used the Rayment et al. model obtained from chicken skeletal myosin S1 (Rayment et al., 1993b) (PDB 2MYS). The starting model for the acto-S1 was that from Rayment et al. (1993a). Further details can be found in Chen et al. (2001).

#### 2.5. Real-space refinement

Because the original acto-S1 models, which incorporated atomic structures obtained by X-ray crystallography, were modified to fit the reconstruction envelope, a considerable number of atom–atom conflicts between domains were introduced in our model building. We therefore used a real-space crystallographic model refinement program, as a vehicle for reducing interdomain conflicts and at the same time produce a quantitative fit to the density (Chen et al., 2001).

The real-space refinement program, RSref, is linked to the TNT crystallographic refinement program (Tronrud et al., 1987), which adds a geometry engine that tests for atom–atom conflicts, from which it adjusts the model to reduce their number and severity (Chapman, 1995). RSref did not improve on the quality of the fit to the density as judged by the correlation coefficient (Chen et al., 2001). However, the manual rebuilding of the initial model introduced a substantial number of atom–atom conflicts. It was the reduction of these atom–atom conflicts that was the primary improvement produced by real-space refinement.

The resolution of the averaged motifs ( $\sim 7$  nm) was too low to resolve the individual actin monomers, making it problematic to infer changes in structure at the actin–myosin interface. Thus, the motor domains were held constant and only the movements of the light chain domain and of the entire actin filament with attached motor domains were quantitatively adjusted when fitting by our procedure. The models were rebuilt using only adjustments of and within the lever arm comprising the converter domain and LCD (i.e., HC residues G710 to K843, ELC, and RLC). For refinement the lever arm was divided into six rigid bodies including

the *converter* (HC residues G710–A769), *LCD1* (HC residues G770–E785), *LCD2* (HC residues I786–A805), *LCD3* (HC residues M806–K843), *ELC*, and *RLC*. A seventh rigid body included the entire 14-subunit actin filament with all the attached myosin motor domains (heavy chain residues 1–709). The  $C_\alpha$  residues of the ends of the several rigid bodies of the heavy chain part of the lever arm were restrained to stay within 0.34 nm at the pivot points to maintain the continuity of the peptide chain but were otherwise permitted to move independently of one another. The movements of the LCD are model dependent and it is likely that a different choice of rigid bodies would produce different results, especially between the converter and LDC-1. Because of the high computational load that occurs during cycles of RSref, it was not possible to test other assignments of rigid bodies.

#### 2.6. Definitions used for determining angular changes

Angular movements of LCD1–3 were determined using the  $C_\alpha$  coordinates of the following heavy chain residues: L772 and R779 of LCD1, L798 and A805 of LCD2, and F814 and N825 of LCD3. These residue pairs follow a line almost parallel to the  $\alpha$ -helix in each heavy chain segment of the LCD. For LCD3 they correspond to the definition used by Corrie et al. (1999) to define the lever axis. In addition, the “hook” axis was taken from the midpoint of F836 and I838 to the midpoint of M832 and L834, also as defined by Corrie et al.

### 3. Results

#### 3.1. General structure of the myac layer

The most useful thin section from IFM is the myac layer, a 25-nm longitudinal section consisting of alternating myosin thick and actin thin filaments. The interposed thin filament occupies a pseudo-dyad position in the unit cell and receives crossbridges from only the two neighboring thick filaments. Therefore, the entire crossbridge participating in force generation is contained within the myac layer, without intrusion of partial crossbridges from other layers. Rigor crossbridges in IFM form a regular array of crossbridge pairs every 38.7 nm, termed double chevrons, which, when complete, consist of two opposed crossbridge pairs.

We produced a total of 25 crossbridge class averages using the hierarchical ascendant classification scheme (Fig. 1). The average number of motifs contained in each class average was 11. This number was determined based on two conflicting considerations. One was the number of plausible crossbridge structures, which could be large because the different periodicities



Fig. 1. Gallery of surface views of the 25 class averages. The class averages are numbered from 0 beginning at the lower lefthand corner and ending with 24 in the upper righthand corner. The class averages that were used for building pseudo-atomic models are 0, 11, 15–23. Each panel is oriented with the Z-disk at the bottom, M-line at the top with the thick filament to the left and right, and actin filament in the middle. “Lead” bridges are labeled “L” and rear bridges are labeled “R.” The accentuation of the triangular shape is somewhat dependent on the contour threshold used to display the reconstruction. In the displays shown here, we chose the contour level to favor connectivity between the thin and thick filaments rather than to accentuate the underlying shape.

of the thick and thin filaments cause variation in crossbridge origin versus actin target. The other consideration was a desire to obtain as much averaging as possible. Eleven of the 25 class averages were used to build pseudo-atomic models. Each of the class averages contained paired lead bridges, but some class averages lacked rear bridges entirely and some had only a single, unpaired rear bridge. One class average contained a two-headed rear bridge and one class average contained a single-headed lead bridge. However, two-headed lead bridges and single-headed rear bridges were the rule.

Direct biophysical and biochemical measurements indicate that ~75% of the available myosin heads in rigor IFM attach to actin (Goody et al., 1985; Lovell et al., 1981; Thomas et al., 1983). If occupancy were 100%, the ratio of all myosin heads to all actin targets (Reedy, 1967) would be 7.1 heads attached per 38.7 nm. Taking the number of motifs contained in each class average and the number of myosin heads modeled per class average yields a head occupancy of 5.44 per class average (i.e., per 38.7 nm). This value is 76% of the predicted maximum and therefore the modeled class averages are representative of the myosin head occupancy in rigor IFM.

### 3.2. Model building

We began our fitting of the IFM rigor crossbridges using a regular 28/13 actin helix 14 monomers long decorated with S1s in the Rayment et al. orientation on the central eight actins. Through manual alignment of this starting model with the density envelope, we picked an orientation in which the axial positions of the S1s fit into the envelopes of the crossbridges in that motif. The extra S1s in the initial model that did not match the position of any crossbridge density were removed from the working database. Despite the low resolution of the reconstruction, each of the class averages for which models were built indicated that the 2.7-nm stagger between crossbridges on opposite sides of the thin filament was preserved. Even with a good initial alignment of the motor domains, it was clear that the LCD lever arms would not fit the bridge envelopes without modification (Chen et al., 2001).

We chose a conservative rebuilding approach by keeping the interaction between myosin and actin constant, modifying only the LCDs. In the lead bridge envelopes this was simple, because the motor domains could be aligned without modification. At the rear bridge, it was often necessary to alter the twist of the actin filament in order to place the motor domain of myosin into the reconstruction envelope without altering the rigor relationship at the actin/myosin interface. The actin filament twist was modified manually by adjusting the rotation between successive actin monomers along the actin helix until all the motor domains of the model fell within the reconstruction envelope. We conserved the 180° twist of the actin filament each 38.7 nm by adjusting the twist in other regions in the opposite direction. This conservation of twist is required to account for the 38.7-nm periodicity of the actin target zones with interposed troponin bumps which reflect a full 180° helical rotation of the thick filament every 38.7 nm axially.

Once the actin filament and the myosin motor domain were positioned within the density envelope, the LCD of the atomic S1 model was rebuilt to fit into the crossbridge density. This was initially done by rotation about G710 as a pivot. However, this introduces many interdomain clashes. When the LCD was divided into several rigid bodies a better fit was obtained, but some interdomain clashes remained. Overall, the repositioning of the LCD used in this rebuilding involved two kinds of adjustment. For two-headed crossbridges, the LCD arm of the Z-ward head was tilted axially *M*-wards and rotated azimuthally counterclockwise to a point midway between the starting *M*-ward and *Z*-ward S1 heads. The LCD of the *M*-ward head was tilted axially *Z*-ward and rotated azimuthally clockwise. These two adjustments brought the C-termini of S1 atomic models in the two-headed crossbridges to nearly the same axial level along the filament axis.

The S2 component of the crossbridges must merge to form an  $\alpha$ -helical coiled-coil but whether this coiling begins at K843 (Cai et al., 1995; Sata et al., 1996) or subsequent to an initial uncoiled segment is unclear (Knight, 1996; Trybus et al., 1997). Given this uncertainty, we converged the S1 C-termini early to allow coiled-coil formation to begin as soon as possible after K843. Taken alone, the axial and azimuthal adjustments would position the “hook” helices (residues P830–K843) of the two S1 heavy chains parallel to each other, with no tendency to merge. To force the convergence required for formation of the coiled-coil, we twisted the LCD of each head toward the other around residue G710 by a similar amount. This left the average “twist” angle close to the original Rayment et al. twist angle. Since we do not resolve the S1–S2 junction and lack independent measures from these reconstructions of the precise angle between S1 and S2 at this junction, the amount and direction of the twisting are hypothetical, but the necessity for convergence is clear. This twist component of our rebuilding correlates with some previously published probe and crosslinking data, as described below.

In surface relief, in longitudinal view, the two-headed rigor crossbridges have an overall triangular shape indicative of two myosin heads originating from a common vertex and binding to adjacent actin monomers (Fig. 2). This compact vertex is a key element forcing realignment of the initial atomic model of acto-S1 (Rayment et al., 1993a). In the Rayment et al. model, the S1 heads are independent structures, free from the common origin that constrains them in the intact molecule. In acto-S1, the C-termini of the myosin heavy chains along successive actins are well separated both axially and azimuthally. However, the S1–S2 junctions of the two heads in each lead bridge must nearly coincide both axially and azimuthally in order to join at the observed common vertex.

The dual-headed structure of the lead bridges, originating from a common origin but binding separate actin monomers, accentuates their triangular shape. The rear bridge density was generally narrower and less tapered than the lead bridge. The taper of rear bridges derives only from the pear shape of a single myosin head.<sup>3</sup>

When all of the refined S1s from two-headed crossbridges are superimposed on a single motor domain (which remained unmodified by our procedure), the positions of K843 of the myosin heavy chains define an

<sup>3</sup> In one class average the rear bridge had a size and shape consistent with a composition of two heads. It was classified as a rear bridge because of its proximity to the troponin density and from the location of its thick filament origin. The front–back rule derived for AMPPNP crossbridges (Schmitz et al., 1996) makes specific predictions of where target zone bridges must originate and in this case, the rule clearly identifies this two-headed crossbridge as a rear bridge.

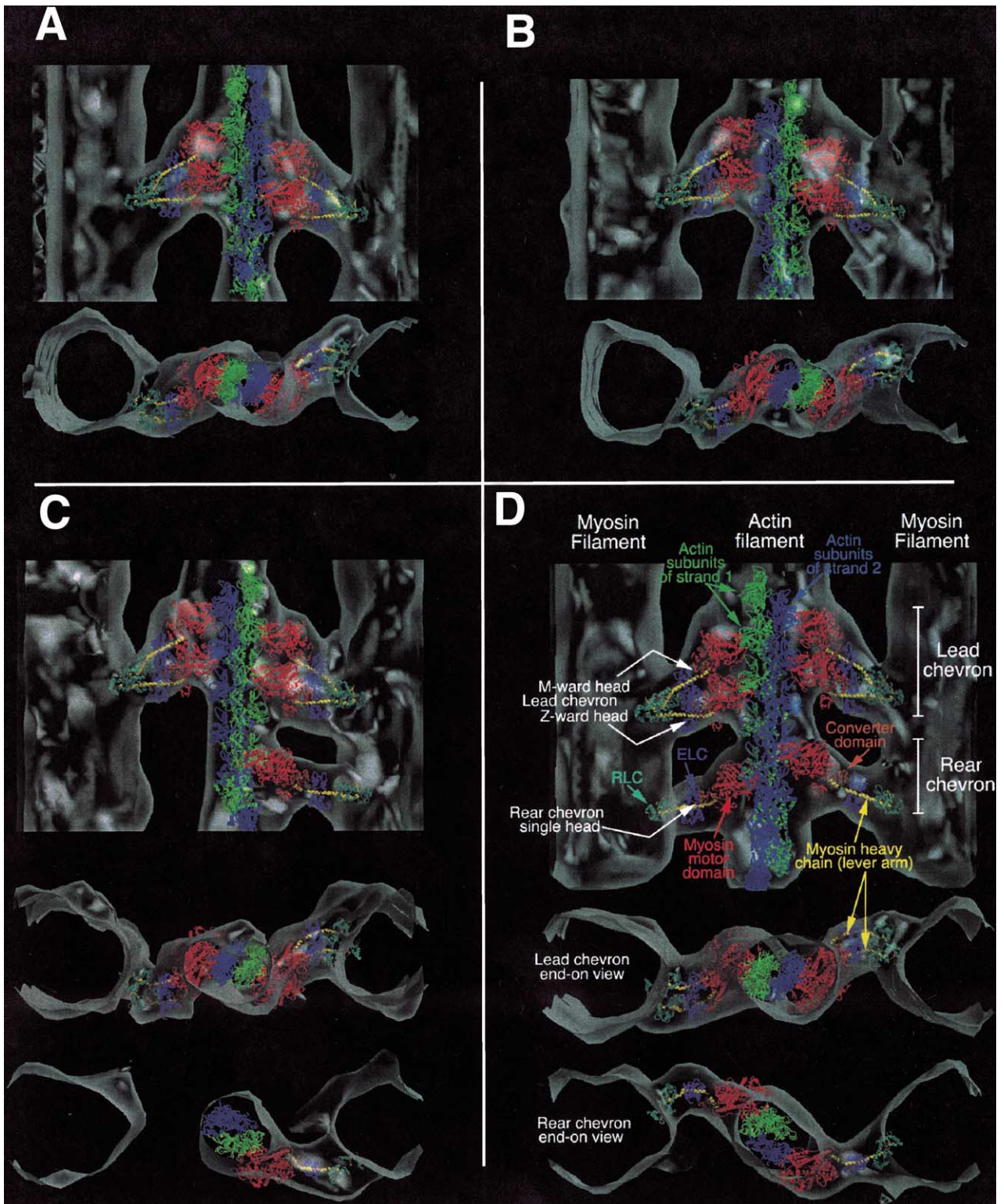


Fig. 2. Atomic models of Rayment–Milligan rigor acto-S1 (protein backbones in color) docked and rebuilt to fit these class-averaged motifs from the 3-D reconstruction (translucent gray envelope). These examples illustrate the final lever arm positions required to fit the crossbridge envelopes. (A) and (B) are models of “single chevrons,” motifs composed only of paired “lead” bridges, each accommodating the two heads from one myosin molecule; (C) is an incomplete double chevron, a motif composed of paired “lead” bridges with an unpaired “rear” bridge; (D) is a complete “classical” double chevron composed of paired “lead” bridges with paired “rear” bridges. The end-on view of lead bridges below shows separation of distal lever arms. The color scheme shows opposite strands of the actin helix in green and blue. The heavy chain in the motor domain to K709 is red. The position of the rigor motor domain on actin has not been modified and is identical for all heads. The heavy chain core throughout the lever arm (G770–K843) is yellow and is embraced by the light chains (ELC in magenta and RLC in cyan). The converter domain is brownish orange: G710–A799. Both bending and twisting of lever arms were required to fit the atomic model to the crossbridges. On our web site at <http://www.sb.fsu.edu/~taylor/lifan/index.html>, each of the models fitted to our class-averaged rigor motifs can be viewed in an animated sequence.

arc that covers an axial range of 5.8 nm. The axial angles of the single-headed crossbridges, all except one of which are rear bridges, covered the same angular range. In projections of longitudinal view, the rear bridges usually appear less angled than lead bridges, largely because of the more uniform and steeper angle of the *M*-ward head of the triangular lead bridges (Taylor et al., 1984).

### 3.3. Relative movements of the domains

The atom–atom conflicts that resulted from the model building were introduced by two kinds of LCD adjustment. The azimuthal rotation and *M*-ward axial adjustment of the LCD for the *Z*-ward heads of each lead bridge tends to drive the converter domain into the heavy chain loop containing residues Q500–F512. This same adjustment was required to fit the rear bridges. For *M*-ward heads, the azimuthal rotation and *Z*-ward adjustment tend to drive the converter domain into loops containing heavy chain residues A92–H98 and helix S79–Y85 and loop E21–D33 at the ends of the SH3 domain. After real-space refinement, some shifts were seen in all of the rigid bodies, but the largest domain shifts were seen at the converter domain. Other shifts were due to the twisting of the light chain domains used to bring them into close proximity at the S1/S2 junction. The other interdomain clash involved the N-terminal lobe of the RLCs at the S1/S2 junction. This overlap was resolved by relaxing the constraint placed on the distance between K843 of the two heads. We also allowed the converter domain ELC and RLC residues to move independently of the LCD1–3 segments of the heavy chain helices to which they are bound as a test of how much relative movement might be produced during refinement.

One set of large movements was generated by rebuilding and subsequent refinement between the converter–LCD1 domain and the ELC–LCD2 domain (Fig. 3A). Averaged over all of the refined S1s, the bend between these two domains averaged  $35.7^\circ \pm 7.9^\circ$  (range  $21.9^\circ$ – $64.6^\circ$ ). This angle measures the total bend, not just the axial bend and compares to a value of  $30.9^\circ$  for the starting Rayment et al. atomic model. Although the range of movement is relatively large over all the models, of the 58 myosin heads in the database, 47 had angles between  $30^\circ$  and  $40^\circ$ . This would imply that the hinge we assumed between LCD1 and LCD2 is relatively rigid.

A second set of interdomain movements involved the ELC–LCD2 domains and the RLC–LCD3 domains (Fig. 3B), all four of which were allowed to move as separate rigid bodies. The average angle between LCD2 and LCD3 was  $44.8^\circ \pm 1.5^\circ$ , which includes three myosin heads from rear bridges that were very different from the other 55. This angle also measures the total bend, not just the bend in the axial direction. This value again

compares with  $36.6^\circ$  for the starting S1 atomic model. LCDs from different sources have different amounts of bend between the ELC and the RLC (Houdusse and Cohen, 1996); the absolute difference between our refined models and the starting Rayment et al. model may indicate a species difference. However, the constancy of the bend in our refined models, as exemplified by the small standard deviation, supports the idea that this portion of the lever arm is a relatively rigid body.

Our assumption that the converter and the LCD1 domain could be independent turned out to allow considerable movement between them during the refinement (Fig. 3C). This is not surprising as the converter movements applied during the initial manual rebuilding introduced the majority of the poor atom–atom conflicts. The simplest way to remove them involved converter domain movements independent of the LCD1  $\alpha$ -helix. Refining LCD1 and the converter in concert as a single rigid body would likely have produced a different refined structure at the catalytic domain–converter domain interface and perhaps a different positioning of the ELC.

We also allowed the ELC and the RLC to refine as separate rigid bodies relative to the heavy chain segments to which they were attached. The resulting movements of the ELC with respect to LCD2 and the RLC with respect to LCD3 were small (Figs. 3D and E).

### 3.4. Orientations of the LCD relative to Corrie et al.

Our refined molecular models of rigor crossbridge forms facilitate quantitative comparison with results from experiments that used bifunctional fluorescent probes attached to the RLC in vertebrate striated muscle (Corrie et al., 1999). These studies measured changes in the orientation of the RLC during active contraction and in rigor. Our particular interest lies in comparing their measurements of the vertebrate rigor state to our rigor models (Table 1).

Corrie et al. measured frog fibers decorated with exogenous S1 and fibers in which exogenous labeled RLC was diffused into the fibers. Their derived value of the lever arm tilt for exogenous S1 in rigor was  $111^\circ$ , while that for endogenous myosin heads was  $108^\circ$ . IFM rigor shows three groups of myosin heads, rear bridges and *M*-ward and *Z*-ward heads of lead bridges (Table 1). For all three head groups, our average overall value of the lever arm tilt, using the Corrie et al. reference values, was  $119^\circ \pm 12^\circ$ . For the *M*-ward head, the average was  $151^\circ \pm 1.1^\circ$  and for the *Z*-ward head the average was  $98^\circ \pm 2.3^\circ$ . For the rear bridges, the value for lever arm tilt was  $106^\circ \pm 12^\circ$ , very close to the Corrie et al., value of  $108^\circ$ . Values for the tilt of the rear bridges are important because they are predominately single headed and their tilt angle is not constrained by a common origin with a companion head attached to actin.

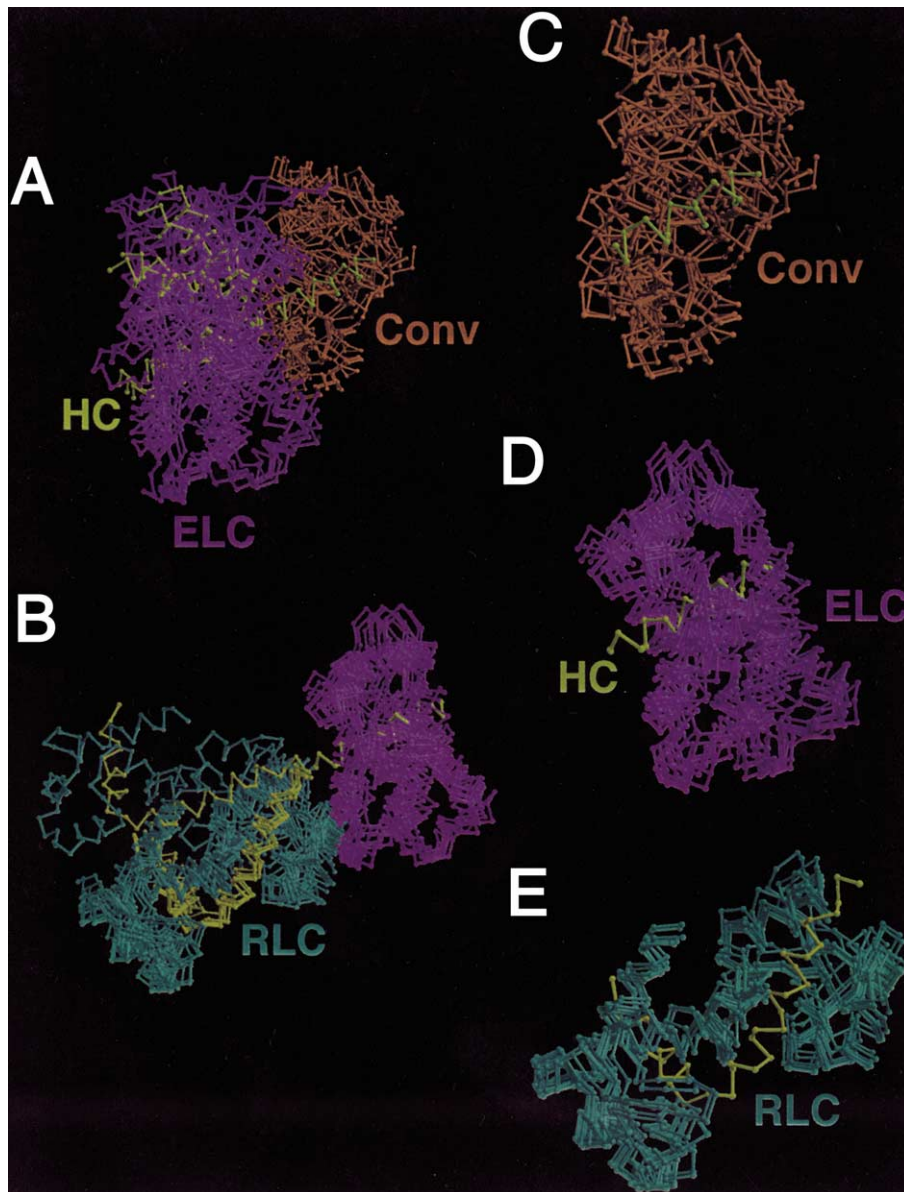


Fig. 3. Views of movements of the different domains relative to the long heavy chain  $\alpha$ -helix of the lever arm. For this figure, a subset of 11 S1s was selected from the 58 total that encompassed as much of the entire range of movement as possible. These images show (A) the converter domain, ELC, and LCD2 aligned relative to LCD1. Although the LCD1 rigid body is shown as fixed, all the rigid bodies shown were allowed to move during the refinement. (B) ELC, RLC, LCD3 aligned relative to LCD2, (C) the converter domains aligned to LCD1, (D) the ELCs aligned to LCD2, (E) the RLCs aligned to LCD3. The color scheme is the same as that for Fig. 2. The entire range of movements can be seen as an animated sequence at our web site at <http://www.sb.fsu.edu/~taylor/lifan/index.html>.

Twist of the lever arm around its own long axis has also been observed and quantified during active contraction of vertebrate muscle (Corrie et al., 1999; Volkmann et al., 2000). We have also measured the twist of the light chain lever arm using the angle of the “hook” at the C-terminus of the S1 (Table 1). In the Rayment et al. atomic structure of isolated S1, the “hook” is inclined  $-9^\circ$  off of the thick filament axis, which is defined as  $0^\circ$ . In contrast, Corrie et al. detected a rigor hook orientation with bifunctional fluorescent probes on the RLC that was  $+29^\circ$  (i.e., in the opposite

direction from Rayment rigor S1). The values for twist angle of the lever arm that we measure differ from both Rayment et al. and Corrie et al. rigor values.

We assumed that S2 extended in roughly the same direction as the “hook.” We also lacked information on the separation between the two heavy chains at the S1–S2 junction. We therefore assumed that the  $C_\alpha$ s of K843 at the C-terminus of S1 should approach within  $\sim 1.8$  nm of each other, the maximum separation that would allow formation of a coiled-coiled in S2. The average lever arm twist required to fit double-headed lead bridges was

Table 1  
Lever arm orientations

	<i>M</i> -ward head	<i>Z</i> -ward head	Rear bridge	Overall	S1 <sup>a</sup>	S1 (exogeneous) <sup>b</sup>	Rigor (vertebrate skeletal) <sup>b</sup>
Lever arm tilt ( $\beta$ )							
Average	151°	98°	106°	119°	111°	111°	108°
SD	1.1°	2.3°	12°	25°		21°	24°
Max	153°	101°	145°	153°			
Min	149°	94°	93°	93°			
Lever arm twist ( $\gamma$ )							
Average	-23°	-1.6°	-11°	-12°	-9°	23°	29°
SD	3.0°	1.2°	14°	12°		25°	29°
Max	-20°	-0.21°	-1.0°	-0.21°			
Min	-29°	-4.2°	-48°	-48°			

<sup>a</sup> From Rayment et al. (1993a).

<sup>b</sup> From Table 1 of Corrie et al. (1999).

$-12^\circ \pm 12^\circ$ , which is different from the Corrie et al. value of  $+29^\circ$ . For *M*-ward heads of lead bridges, the twist value was  $-23^\circ \pm 3^\circ$  and for *Z*-wards heads, the twist value was  $-1.6^\circ \pm 4^\circ$ . The difference reflects the twisting of the *M*-ward and *Z*-ward heads toward each other but maintaining the same average direction as the Rayment et al. rigor model. Close approach of the K843 could have been achieved by a combination of different amounts or directions of twist of each head, because the bridge envelope did not stringently constrain the amount or direction of twist to fit the model within the bridge. Rear bridges, which were generally single headed, did not require significant alteration of twist and so their average twist is similar to that of the Rayment et al. starting model.

### 3.5. Crosslinking distances

We determined the distance from several of the sites where Wu et al. (1999) introduced cystein mutations to the nearest residue on the partner head in our atomic models of two-headed rigor crossbridges. We used the homologous residues in the chicken skeletal muscle RLC for these calculations. Thus, residues Q15, A23, S59, C108, and T134 of the smooth muscle RLC correspond to A9, S17, A53, V103, and T129 of the skeletal muscle RLC. In the following description, we refer to the residues by their smooth muscle equivalents. Note that Q15 and A23 (smooth muscle) have no corresponding residues visible in the RLC of the Rayment et al. starting model of chicken skeletal muscle. However, in place of A23, we have used residue F24 to compare crosslinking distances (see Fig. 4).

IFM two-headed rigor crossbridges are asymmetric so that only one of the two cystein mutation sites would be in a position to crosslink to the other RLC residue. For example, the S59 C $\alpha$  on the *M*-ward head is well placed to crosslink to the *Z*-ward head RLC, but the S59 C $\alpha$  on the *Z*-ward head is too distant to crosslink to the *M*-ward RLC. On the *Z*-ward head both C108 and F24

are relatively well placed to crosslink to the *M*-ward head, but the corresponding residue on the *M*-ward head is not positioned to crosslink to the *Z*-ward head. The T134 C $\alpha$ s on either head are not positioned for crosslinking because for the most part, they are located to the side opposite the companion RLC.

C108, a wild-type residue, is  $1.25 \pm 0.08$  nm from the *M*-ward head RLC in our atomic models, which seems too far to be bridged by the 0.89-nm crosslinker. Wu et al. observed crosslinking at C108 when smHMM was bound to actin in rigor. In several of the models, C108 is close to the C-terminus of the *M*-ward head. In smooth muscle, the RLC has two additional residues at the C-terminus that are not found in the skeletal muscle RLC. The additional residues in smHMM may bridge the gap, thereby reconciling the crosslinking result with our rigor models.

Wu et al. investigated a site on the N-terminal peptide of the RLC (A23C) that can be crosslinked to the RLC of the second head when bound to actin regardless of the state of RLC phosphorylation. The topology of our two-headed crossbridges shows that the neighboring residue, F24, is 0.77 nm from the RLC of the *M*-ward head. This would make crosslinking observed through A23C very probable in the rigor two-headed crossbridge.

The S59C smRLC cysteine mutation site was very sensitive to the state of phosphorylation when smHMM was bound to actin. Wu et al. found that the S59C would crosslink to the companion RLC when smHMM is dephosphorylated, but not when bound to actin in the phosphorylated state. In our rigor IFM pseudo-atomic models, the S59 C $\alpha$  is  $1.03 \pm 0.16$  nm from the nearest residue on the companion RLC, a marginal distance for crosslinking, possibly making the site a sensitive indicator of changes in myosin head structure.

## 4. Discussion

The rigor structures described here were derived by a new procedure that comprises (1) electron tomography

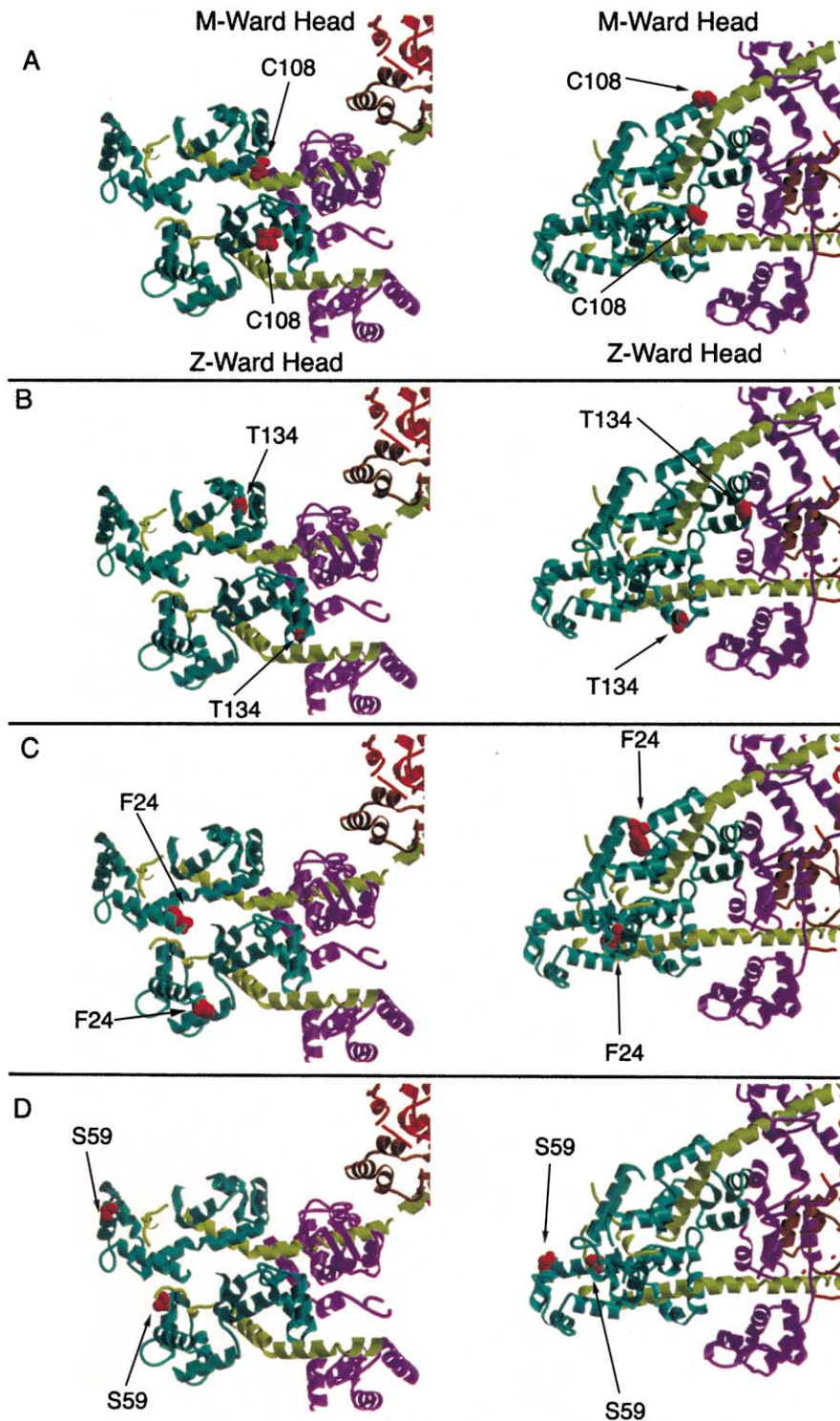


Fig. 4. Locations of the crosslinked residues from Wu et al. Figures in the lefthand column are viewed down the filament axis. Figures in the righthand column are viewed perpendicular to the filament axis. The *M*-ward S1 is at the top and the *Z*-ward S1 is at the bottom. The color scheme for the polypeptide chains, which are shown as ribbon diagrams, is the same as that for Fig. 2. Mutated residues are shown in red as space filling spheres. (A) Locations of C 108 (smooth muscle residue), (B) Locations of T134C, (C) Locations of F24C, (D) Locations of S59C.

to obtain a 3-D image that does not involve spatial averaging, (2) multivariate statistical analysis (correspondence analysis) which identified motifs having

similar structure so that they could be combined to form class averages, and (3) use of a quantitative fitting and refinement procedure which had the effect of reducing

poor atom–atom contacts introduced by the initial manual model building. The limited resolution of the reconstruction and the novelty of the approach require independent evaluation of the result using data from the literature that speak to the quality of the models. These data come from several sources, both spectroscopic and biochemical.

#### 4.1. Orientations and movements of the LCD

Our pseudo-atomic models of rigor crossbridges facilitate comparison with other experimental observations on domain orientations made with other techniques, as long as those techniques refer their measurements to an atomic coordinate frame. Thus, we were able to correlate our models with spectroscopic measurements of RLC orientation, most of which were made after our models were built and refined. The results of Corrie et al. (1999) are particularly informative because their use of a bifunctional probe allows such a direct comparison. Comparison of light chain domain tilt for rigor crossbridges in vertebrate striated muscle indicate an average orientation of  $\beta = 108^\circ$  ( $\sigma = 24^\circ$ ). Our value for rigor IFM derived from microscopy is  $\beta = 119^\circ$  ( $\sigma = 25^\circ$ ). However, because our measurements are made from individual myosin heads, our results show a distinct bimodal character. We do not think that our results overall differ significantly from those of Corrie et al. given the wide variance of their numbers and ours. However, our somewhat greater value may be an indication of some section compression which might serve to increase the average tilt of the crossbridges.

More recently, Hopkins et al. (in press) using a bifunctional probe attached to different regions of the RLC have examined alterations in the tilt and twist of the RLC. They defined the axes differently, using the entire lever arm, including the converter from C704 to K843, instead of just the RLC domain. Their value for tilt in this coordinate frame for S1 (from Rayment et al., 1993a) is  $\beta = 102.2^\circ$  and for rigor is  $\beta = 80^\circ$  and our value in this frame is  $\beta = 100^\circ$  ( $\sigma = 14^\circ$ ). Again, our higher value may be an indicator of some section compression.

Recently, Baumann et al. (2001) measured the mobility of probes attached to the ELC and to the RLC in synthetic myosin filaments. Close correlation between the mobilities under different conditions indicate that the ELC and RLC domains were rigid relative to each other. The average angular difference of  $4^\circ$  between ELC and RLC domains derived from their measurements corresponds well to the standard deviation of  $3.7^\circ$  derived from our reconstructions.

#### 4.2. RLC–RLC crosslinking

Our refined models for the two-headed crossbridge in rigor muscle facilitates interpretation of previous

crosslinking results on smHMM bound to actin with and without phosphorylation (Wu et al., 1999). Note that the crosslinker has a length of 0.89 nm, whereas the distance measured in our models is from the  $C_\alpha$  to the  $C_\alpha$  of the nearest residue. The actual distance may be more or less than that depending on the orientation of the side chains.

Our results are in general agreement with the crosslinking data of Wu et al. Their data for actin-bound smHMM show that the T134C mutation would not crosslink under any circumstances and our model for the two-headed rigor crossbridge shows that for both heads the T134C mutation is well removed from the RLC of the companion head. Wu et al. observed crosslinking through C108 independently of RLC phosphorylation. In our rigor two-headed crossbridge C108 is  $\sim 1.2$  nm from the companion RLC but close to the C-terminus, where two additional residues in the smooth muscle RLC could shorten the crosslinking distance. Wu et al. observed that mutation A23C crosslinked to the second RLC under all conditions tested and our two-headed crossbridges shows that the neighboring residue, F24, is 0.77 nm from the RLC of the *M*-ward head. This would make crosslinking observed through A23C very probable in the actin-bound rigor state.

The S59C residue seems to be located at a position that makes it very sensitive to the state of RLC phosphorylation. Wu et al. found that when bound to actin in the rigor state, S59C could be crosslinked to the companion RLC only when the RLC was not phosphorylated; S59C would not crosslink when the RLC was phosphorylated. In our two-headed rigor models, S59 of the *M*-ward head is located at the interface of the two heads,  $\sim 1.03$  nm from the companion RLC. Our models suggest that this location makes S59C a very sensitive probe for small changes in the separation between the two S1s that may be induced by phosphorylation.

#### 4.3. Adaptability to other biological systems

The methodology described here has been developed for the purpose of analyzing disordered structures within an ordered lattice and specifically for application to muscle. Can these methods be adapted to other systems? Muscle is an ideal specimen for this work because it is ordered in 3-D and each tomogram yields large numbers of motifs which have a highly regular component, the actin filament, together with a disordered component, the crossbridges. This disorder made it essential to adapt to 3-D motifs the image classification methods that have been so successful for classifying 2-D projections. One limitation to the classification is a method for estimating the number of classes present within the data set. In the present case, this was “guessed” but the guesswork may be eliminated through the

use of self-organizing maps described elsewhere in this issue (Pascual-Montano et al., 2002).

Our method also incorporates a real-space refinement procedure to quantitatively fit the models to the reconstructions. This procedure relies on having atomic models for the various components. In cases where all the reconstruction data come from images, there is no particular advantage to using a Fourier-based method. An advantage of real-space refinement is the opportunity to modify a component of the structure, which may contribute in a small way to the overall structure but which is localized and readily identifiable. In our case, this is the light chain domain. Since we had to modify the original X-ray model to fit the density, some refinement procedure was warranted to both quantify the fit to the density and to improve the stereochemistry in locations where domains were superimposed.

Correspondence analysis and real-space refinement are completely general methods for structural analysis. Any atomic model can be refined in real space and any collection of refined images can be classified, whether they are 2-D or 3-D. The adaptation of these methods to other systems is likely to depend on the number of motifs that can readily be obtained in a tomogram and whether they have a component present in each motif that is ordered even in the presence of a component that is disordered. Many partially ordered biological systems exist that have been studied over the years. These include decorated actin filaments, decorated microtubules, other muscle types, such as skeletal, cardiac, and smooth muscle, and essentially any other system where some order underlies a disordered structure. The procedures described here or adaptations of them may make these systems tractable to structural analysis.

## Acknowledgments

The authors thank Mr. Gary Connors for his help with the figures. The PDS1010M was purchased with funds from NSF Grant PCM-8400167. This research was supported by NIH Grants GM30598 and AR14317.

## References

- Baumann, B.A., Hambly, B.D., Hideg, K., Fajer, P.G., 2001. The regulatory domain of the myosin head behaves as a rigid lever. *Biochemistry* 40, 7868–7873.
- Cai, S., Ferguson, D.G., Martin, A.F., Paul, R.J., 1995. Smooth muscle contractility is modulated by myosin tail-S2-LMM hinge region interaction. *Am. J. Physiol. Cell Physiol.* 269, C1126–C1132.
- Chapman, M.S., 1995. Restrained real-space macromolecular atomic refinement using a new resolution-dependent electron-density function. *Acta Crystallogr. A* 51, 69–80.

- Chen, L.F., Blanc, E., Chapman, M.S., Taylor, K.A., 2001. Real space refinement of acto-myosin structures from sectioned muscle. *J. Struct. Biol.* 133, 221–232.
- Corrie, J.E., Brandmeier, B.D., Ferguson, R.E., Trentham, D.R., Kendrick-Jones, J., Hopkins, S.C., van der Heide, U.A., Goldman, Y.E., Sabido-David, C., Dale, R.E., Criddle, S., Irving, M., 1999. Dynamic measurement of myosin light-chain-domain tilt and twist in muscle contraction. *Nature* 400, 425–430.
- Frank, J., van Heel, M., 1982. Correspondence analysis of aligned images of biological particles. *J. Mol. Biol.* 161, 134–137.
- Goody, R.S., Reedy, M.C., Hofmann, W., Holmes, K.C., Reedy, M.K., 1985. Binding of myosin subfragment 1 to glycerinated insect flight muscle in the rigor state. *Biophys. J.* 47, 151–169.
- Holmes, K.C., Popp, D., Gebhard, W., Kabsch, W., 1990. Atomic model of the actin filament. *Nature* 347, 44–49.
- Hopkins, S.C., Sabido-David, C., Heide, U.A.v.d., Ferguson, R.E., Brandmeier, B.D., Dale, R.E., Kendrick-Jones, J., Corrie, J.E.T., Trentham, D.R., Irving, M., Goldman, Y.E., in press. Orientation changes of the myosin light chain domain during filament sliding in active and rigor muscle. *J. Mol. Biol.*
- Houdusse, A., Cohen, C., 1996. Structure of the regulatory domain of scallop myosin at 2 Å resolution: implications for regulation. *Structure* 4, 21–32.
- Jones, T.A., Zou, J.-Y., Cowan, S.W., Kjeldgaard, M., 1991. Improved methods for building protein models in electron density maps and the location of errors in these models. *Acta Crystallogr. A* 47, 110–119.
- Knight, P.J., 1996. Dynamic behaviour of the head–tail junction of myosin. *J. Mol. Biol.* 255, 269–274.
- Lovell, S.J., Knight, P.J., Harrington, W.F., 1981. Fraction of myosin heads bound to thin filaments in rigor fibrils from insect flight and vertebrate muscles. *Nature* 293, 664–666.
- Pascual-Montano, A., Taylor, K.A., Winkler, H., Pascual-Marqui, R.D., Carazo, J.-M., 2002. Quantitative self-organizing maps for clustering electron tomograms. *J. Struct. Biol.* 138, 114–122.
- Rayment, I., Holden, H.M., Whittaker, M., Yohn, C.B., Lorenz, M., Holmes, K.C., Milligan, R.A., 1993a. Structure of the actin–myosin complex and its implications for muscle contraction. *Science* 261, 58–65.
- Rayment, I., Rypniewsky, W.R., Schmidt-Bäse, K., Smith, R., Tomchick, D.R., Benning, M.M., Winkelmann, D.A., Wesenberg, G., Holden, H.M., 1993b. Three-dimensional structure of myosin subfragment-1: a molecular motor. *Science* 261, 50–58.
- Reedy, M.K., 1967. Cross-bridges and periods in insect flight muscle. *Am. Zool.* 7, 465–481.
- Reedy, M.K., Reedy, M.C., 1985. Rigor crossbridge structure in tilted single filament layers and flared-X formations from insect flight muscle. *J. Mol. Biol.* 185, 145–176.
- Sata, M., Matsuura, M., Ikebe, M., 1996. Characterization of the motor and enzymatic properties of smooth muscle long SI and short HMM: role of the two-headed structure on the activity and regulation of the myosin motor. *Biochemistry* 35, 11113–11118.
- Schmitz, H., Reedy, M.C., Reedy, M.K., Tregear, R.T., Winkler, H., Taylor, K.A., 1996. Electron tomography of insect flight muscle in rigor and AMPPNP at 23 °C. *J. Mol. Biol.* 264, 279–301.
- Taylor, K.A., Reedy, M.C., Córdova, L., Reedy, M.K., 1984. Three-dimensional reconstruction of rigor insect flight muscle from tilted thin sections. *Nature* 310, 285–291.
- Taylor, K.A., Reedy, M.C., Córdova, L., Reedy, M.K., 1989a. Three-dimensional image reconstruction of insect flight muscle. I. The rigor myac layer. *J. Cell Biol.* 109, 1085–1102.
- Taylor, K.A., Reedy, M.C., Córdova, L., Reedy, M.K., 1989b. Three-dimensional image reconstruction of insect flight muscle. II. The rigor actin layer. *J. Cell Biol.* 109, 1103–1123.
- Taylor, K.A., Reedy, M.C., Reedy, M.K., Crowther, R.A., 1993. Crossbridges in the complete unit cell of rigor insect flight muscle

- imaged by three-dimensional reconstruction from oblique sections. *J. Mol. Biol.* 233, 86–108.
- Taylor, K.A., Tang, J., Cheng, Y., Winkler, H., 1997. The use of electron tomography for structural analysis of disordered protein arrays. *J. Struct. Biol.* 120, 372–386.
- Thomas, D.D., Cooke, R., Barnett, V.A., 1983. Orientation and rotational mobility of spin-labelled myosin heads in insect flight muscle in rigor. *J. Muscle Res. Cell Motil.* 4, 367–378.
- Tronrud, D.E., Ten Eyck, L.F., Mathews, B.W., 1987. An efficient general-purpose least-squares refinement program for macromolecular structures. *Acta Crystallogr. A* 43, 489–501.
- Trybus, K.M., Freyzon, Y., Faust, L.Z., Sweeney, H.L., 1997. Spare the rod, spoil the regulation: necessity for a myosin rod. *Proc. Natl. Acad. Sci. USA* 94, 48–52.
- Unser, M., Trus, B.L., Steven, A.C., 1987. A new resolution criterion based on spectral signal-to-noise ratios. *Ultramicroscopy* 23, 39–51.
- van Heel, M., 1984. Multivariate statistical classification of noisy images (randomly oriented biological macromolecules). *Ultramicroscopy* 13, 165–184.
- van Heel, M., Frank, J., 1981. Use of multivariate statistics in analysing the images of biological macromolecules. *Ultramicroscopy* 6, 187–194.
- Volkman, N., Hanein, D., Ouyang, G., Trybus, K.M., DeRosier, D.J., Lowey, S., 2000. Evidence for cleft closure in actomyosin upon ADP release. *Nat. Struct. Biol.* 7, 1147–1155.
- Winkler, H., Taylor, K.A., 1999. Multivariate statistical analysis of three-dimensional cross-bridge motifs in insect flight muscle. *Ultramicroscopy* 77, 141–152.
- Wu, X., Clack, B.A., Zhi, G., Stull, J.T., Cremo, C.R., 1999. Phosphorylation-dependent structural changes in the regulatory light chain domain of smooth muscle heavy meromyosin. *J. Biol. Chem.* 274, 20328–20335.